Journal of Applied Physics ARTICLE scitation.org/journal/jap

Trajectory deflection of spinning magnetic microparticles: The Magnus effect at the microscale

Cite as: J. Appl. Phys. **127**, 194702 (2020); doi: 10.1063/1.5145064
Submitted: 17 January 2020 · Accepted: 25 April 2020 ·
Published Online: 20 May 2020

M. Solsona,[1,a)] H. Keizer,[1] H. L. de Boer,[1] Y. P. Klein,[2] W. Olthuis,[1] L. Abelmann,[3] and A. van den Berg[1]

AFFILIATIONS

[1]BIOS-Lab on a Chip Group, MESA+ Institute for Nanotechnology, Max Planck-University of Twente Center for Complex Fluid Dynamics, University of Twente, Drienerlolaan 5, Enschede, 7522 NB, The Netherlands
[2]Mesoscale Chemical Systems Group, MESA+ Institute for Nanotechnology, University of Twente, Drienerlolaan 5, Enschede, 7522 NB, The Netherlands
[3]KIST Europe, Saarland University, 66123, Saarbrücken, Germany

[a)]**Author to whom correspondence should be addressed:** miguel.solsona.alarcon@gmail.com

ABSTRACT

The deflection due to the Magnus force of magnetic particles with a diameter of 80 μm dropping through fluids and rotating in a magnetic field was measured. With the Reynolds number for this experiment around 1, we found trajectory deflections of the order of 1°, in agreement with the measurement error in theory. This method holds promise for the sorting and analysis of the distribution in magnetic moment and particle diameter of suspensions of microparticles, such as applied in catalysis, or objects loaded with magnetic particles.

I. INTRODUCTION

A rotating object moving through a medium experiences a Magnus force that is perpendicular to both the axis of rotation and the direction of motion.[1] This effect is well known in ball sports, for instance, as topspin in tennis. The Magnus force is an inertial effect and therefore is most effective for large objects moving at high velocity, such as soccer balls[2] or planets forming in a proto-planetary disk.[3] In these situations, the flow is normally turbulent, characterized by much higher linear (R_e) and rotational Reynolds number (R_o). In this paper, we investigate the Magnus force for laminar flow conditions, at Reynolds numbers close to unity. The experiments were performed with spheres of only 80 μm in diameter, rotating less than five revolutions per second and moving at about 1 cm/s through water.

The Magnus force has technological relevance, since it can be used for magnetic separation of microparticles.[4] In contrast to magnetic separation by force gradients, Magnus separation is performed in a uniform field. The Magnus force separates primarily on particle size, since the deflection of the particles is proportional to the square of their diameter. When increasing the rotation frequency of the field, particles with low magnetic moment can no longer follow the field. So by tuning the rotation frequency, one can independently separate on magnetic moment as well.

The theory of the Magnus effect at low R_e has been studied in detail.[5] It was shown that the Magnus force is linearly proportional to the rotation up to values in the order of 100. However, measurements of the Magnus force are not reported for values below a few hundred.[4] A serious experimental complication is that the deflection of the trajectory of the objects approaches very low values, which complicates analysis. The solution we chose is to reduce the particle size, which also allows us to benefit from microfluidic systems.

Microfluidic technologies have been used extensively to sort cells and microparticles using forces that are a function of combinations of particle properties such as size,[6,7] shape, density,[8] permittivity, susceptibility, and magnetic moment.[9–14] The use of these forces in well-controlled laminar fluids with external actuators enables important applications such as sorting of cancer cells[15]

or catalyst particles.[16] In addition to forces, torque can be applied on particles by rotating fields.[17] At low R_e, linear and angular drag forces are balanced by the applied torque immediately, resulting in constant linear and angular velocity[18–20] and, therefore, a constant Magnus force.

In the experiment we present here, the force resulting in linear velocity was provided by gravitation, and the torque leading to angular velocity was provided by a rotating magnetic field acting on anisotropic magnetic Janus particles with a diameter of 80 μm. These particles are in the same size range as catalyst particles,[16,21] so that the results are of immediate technological relevance. The resulting deflection of the particles was observed by a microscope at different rotation speeds and medium viscosities and compared to an approximate model for low R_e.

We show that if the experiment is performed carefully, the Magnus force can still be observed for R_e around unity and that particle trajectories can be predicted by the Rubinow and Keller model. Since there are no unexpected small-size effects, these results encourage the application of Magnus separation at the microscale using microfluidic technology.

II. THEORY

A sphere dropping through a fluid experiences drag forces on its surface. If the velocity is sufficiently low, the relative velocity of the fluid molecules at the surface is zero, and all drag forces are due to shear between the molecules in the fluid itself. At low velocity, the drag force on a small surface element is proportional to the relative velocity of the fluid at a small distance from that surface. The velocity of the sphere reaches a maximum when the total drag force integrated over the surface is balanced by the gravitational force.

If the sphere does not rotate, the fluid velocity is mirror symmetric to the vertical axis (the falling direction). All horizontal components of the drag forces compensate each other, and all vertical forces add up to a net drag force opposite to the velocity [Fig. 1(a)]. If the sphere rotates, the velocity field is modified. At very low rotation velocity, the field is mirror symmetric with respect to the horizontal plane through the center of the sphere. All horizontal components of the drag forces above the plane are compensated by opposite horizontal forces below that plane. As a result, there is no net horizontal force [Fig. 1(b)]. At higher rotation velocities, however, the fluid approaching the bottom of the sphere (the front side) needs a non-negligible distance to accelerate. At the top of the sphere (the back side), the fluid needs a certain distance to decelerate. As a result, the symmetry with respect to the horizontal plane is lost. Horizontal drag force components above the horizontal plane are no longer compensated by components below that plane. Consequently, there is a net drag force component perpendicular to the vertical axis, and the sphere trajectory is deflected from the vertical axis [Fig. 1(c)].

This resulting force was initially discovered by Isaac Newton and two centuries later again by Magnus.[1] In essence, it is an inertial effect[22,23] and, therefore, increases with increasing linear Reynolds number ($R_e = 2ur/\upsilon_f$) and rotational Reynolds number ($R_o = \Omega r^2/\upsilon_f$), where u (m s^{-1}) is the relative linear velocity between the particle and the fluid, Ω (rad s^{-1}) is the angular velocity [in the experimental part, we express the angular velocity in the more intuitive units of revolutions per second (rps)}, r (m) is the radius of the particle, and υ_f is the kinematic fluid viscosity of the fluid (m^2 s^{-1}).[24,25] Many studies have been performed in order to model this force.[26] For low Reynolds numbers, Rubinow and Keller[5] model the force as

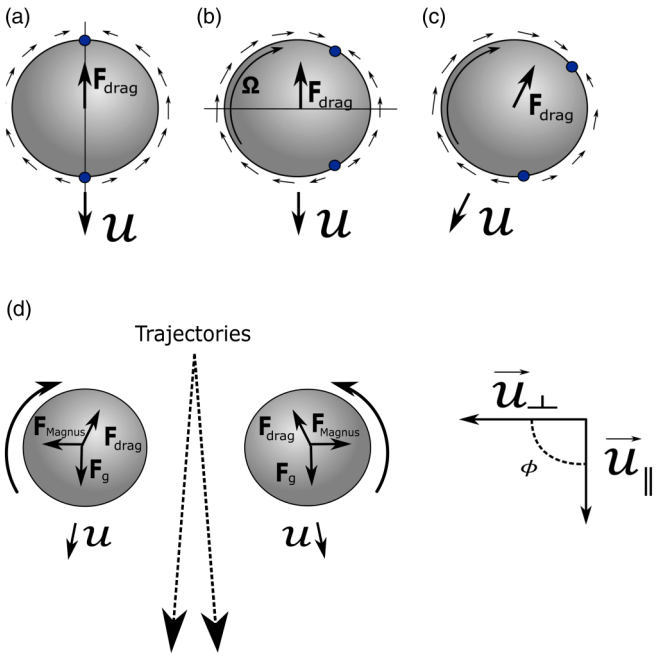

FIG. 1. Schematic drawing of the principle causing the Magnus force. A sphere dropping through a fluid experiences a drag force due to the shear force between the fluid and the sphere surface. The blue dots indicate the point where the relative fluid velocity along the surface of the sphere is zero. (a) When the sphere does not rotate, the vertical axis is an axis of mirror symmetry (indicated by the line). (b) When the sphere rotates slowly, the flow pattern shifts but remains symmetric with the horizontal plane (indicated as well). There is no net force perpendicular to the falling direction. (c) At higher rotation velocity, the fluid at the front side of the sphere needs a certain distance to accelerate, which shifts the position of zero velocity down. The resulting asymmetry in the pattern leads to a tilt in the drag force. (d) Definition of forces and particle trajectories depending on the rotation direction and velocities.

$$F_{magnus} = \pi\rho_f r^3 \Omega \times u, \tag{1}$$

where ρ_f (kg m^{-3}) is the fluid density. The force is maximum when the rotation axis is perpendicular to the relative velocity.

Previous work has experimentally demonstrated the existence of the Magnus force at low R_e. Oesterle and Dinh[27] used metal spheres that were a few centimeters big, attached to a thread in order to spin them, to quantify the Magnus force at R_e between 10 and 140. Others[3,4,28] studied the phenomena at higher R_e, from 300 to 10^5. To the best of our knowledge, the study of the Magnus force has never been performed at Reynolds numbers close to unity. Neither are we aware of studies with microparticles. Experiments with microparticles are challenging, since the Magnus force has a

third-order dependency on the particle size [Eq. (1)], so the deflection decreases considerably with reduction in particle diameter.[29]

In order to rotate the particles, a rotating magnetic field was used so that we can apply a torque over a large spatial region.[17] The Magnus force is proportional to the rotation of the particles [Eq. (1)]. The angular velocity is equal to the rotation of the magnet only if the particles can follow the magnetic field. If the magnet rotation speed is too high, the particles only wobble. To estimate the maximum rotation speed, we assume that the particle has a remanent magnetic moment m_p (A m^2) and that the magnetic field B (T) is small compared to the saturation field. Under these conditions, we can estimate the maximum torque from

$$\Gamma \leq m_p \times B. \tag{2}$$

A sphere with radius r rotating in a fluid with viscosity μ_f (Pa s) at an angular velocity Ω (rad s^{-1}) experiences a drag torque in the direction opposite to the rotation,[30]

$$\Gamma_d = -8\pi r^3 \mu_f \Omega. \tag{3}$$

By balancing the magnetic and angular drag torques, we obtain the maximum angular velocity

$$\Omega \leq \frac{m_p}{r^3}\frac{B}{8\pi\mu_f}. \tag{4}$$

In addition to being pulled sideways by the Magnus force, the particles are pulled downward by gravity as

$$F_g = (\rho_p - \rho_f) g V_p, \tag{5}$$

where ρ_p (kg m^{-3}) is the particle mass density, g (m s^{-2}) is the gravitational acceleration constant, and V_p (m^3) is the volume of the particle. A sphere moving in a fluid encounters a translational drag force in the opposite direction to the movement,

$$F_d = -6\pi r \mu_f u. \tag{6}$$

Balancing the forces, and considering that the magnetic torque is applied perpendicular to g, we obtain the velocity of the particle, which we decompose into the translational and perpendicular components (see Fig. 1),

$$u_{\parallel} = \frac{(\rho_p - \rho_f) g V_p}{6\pi\mu_f r}, \tag{7}$$

$$u_{\perp} = \frac{\rho_f r^3 \Omega u_{\parallel}}{6\mu_f r}. \tag{8}$$

The tilt angle of the trajectory is, therefore,

$$\phi = \tan^{-1}\left(\frac{u_{\perp}}{u_{\parallel}}\right) = \tan^{-1}\left(\frac{\rho_f r^2}{6\mu_f}\Omega\right) = \tan^{-1}\left(\frac{r^2}{6\nu_f}\Omega\right) \approx \frac{r^2}{6\nu_f}\Omega. \tag{9}$$

The approximation is valid for small angles. When the angular speed is zero, the particles follow the gravitational force and the tilt angle is zero. The tilt angle increases with increasing sphere radius r and decreases with increasing kinematic fluid viscosity ν_f (m^2 s^{-1}).

Small particles with high magnetic moment can rotate faster than big particles with low moment [Eq. (4)]. The tilt angle is, however, only dependent on the particle size [Eq. (9)]. So by selecting combinations of rotating speed Ω and field strength B, and filtering out certain tilt angles, we have a method to discriminate particles based on radius to some extent irrespective of the magnetic moment.

Next to the Magnus force, the particles will experience a magnetic force along the magnetic field gradient,

$$F_m = m_p \nabla B, \tag{10}$$

which will also lead to a tilt angle. Fortunately, since the magnetic moment will align with the field direction, the direction of the gradient is independent of the sign of the field. The sign of the tilt angle, however, is determined by the rotation direction. So by measuring both rotations, any tilt due to a magnetic force gradient can be subtracted.

III. MATERIALS AND METHODS

There are three requirements that the fluidic system must meet. First, due to the small deviations expected by the Magnus force and in order to facilitate the following trajectory measurement, the particles should start at very similar positions. Second, the system should be long enough to track long trajectories, and third, the particles should be clearly visible through the fluidic system walls. Figure 2 shows the 3D printed fluidic system with thee inlets and one outlet. Two of the three inlets are used to introduce the liquid, and the third inlet is used to introduce the magnetic particles, also see Fig. S1(a) in the supplementary material. The chamber is 7 cm long and 0.5 cm wide and deep. In order to observe the particles and seal the chamber, a glass slide was glued on the front part of the chip [see Fig. S1(a) in the supplementary material]. To maximize the deflection caused by the Magnus force, the time of the particles inside the chamber should be increased. Therefore, the system will be used with no-flow conditions, letting the particles sink from the inlet to the outlet of the chamber. A very similar particle starting point inside the fluidic system is crucial due to the small deflection expected caused by the Magnus force. Normally, liquid flow or magnetic, electric, or acoustic fields are used to focus the particles inside a microfluidic channel. However, due to the no-flow conditions and the trouble of introducing actuators inside the 3D printed chip, a new method to focus the particles at the same position was developed. Figure 2(c) shows a cut of the particle's inlet of the microfluidic chip where a zig-zag inlet can be seen. As can be seen in Fig. S2 in the supplementary material, particles were rolling downward. Although some of the particles started at very similar positions, this varied due to its large sensitivity on other factors such as the amount of particles arriving to the big chamber at the same time and disturbing each other or by any small flow perturbation caused by the pipetting of the particles inside the inlet.

In order to rotate the particles and avoid any attraction to the magnets, the magnetic field that is used should be as strong and

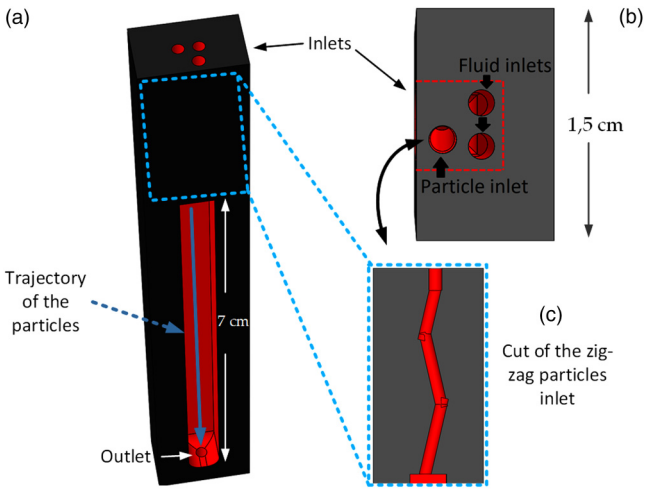

FIG. 2. (a) Schematic drawing of the fluidic chip showing the three inlets and chamber where the particles rotate, (b) the three inlets, and (c) a cut of the zig-zag particles inlet.

homogeneous as possible. Therefore, bigger magnets providing less gradients over the observation area are better than smaller magnets. Also, by placing another magnet on the opposite side of the fluidic chip, the gradient and, therefore, its magnetic force toward the magnets will be reduced (see Fig. 3). Eight N42 magnets, 1 cm wide, 4 cm deep, 1 cm long, and a magnetization of 1.3 T along the longest side, were purchased from Supermagnete.[31] Each rotating arm consisted of four magnets, as can be seen in Fig. S3(b) in the supplementary material. The field strength in the center between the magnets was 122 ± 5 mT. In order to observe the particle's trajectory, a silicon wafer acting as a mirror was glued at a 45° angle to the fluidic system's wall [see Figs. S1(b) and S1(c) in the supplementary material].

Both magnets should rotate at the same speed in order to avoid magnetic field distortion, but due to the fluidic connections and tubing, both magnets could not be attached together. Therefore, a new mechanical system was developed to rotate both magnets at the same speed. Figure S3(a) in the supplementary material shows the system consisting of an electrical motor (Crouzet DC motor, model 820580002) and a gear box with a reduction ratio of 3.4 [see Fig. S1(b) and S1(c) in the supplementary material]. Also, for security reasons, a new system was developed to mount the magnets in the rotating arms. As can be seen in Fig. S3(b) in the supplementary material, first the magnets were stuck together with a separator in the middle and subsequently attached together to one of the rotator's arms. Thereafter, the other rotating arm was brought closer and connected to the second magnet's support, which allows safe separation of both magnets. The magnets repelled each other due to their configuration; therefore, the second arm was pushed away by the magnets. The separation of the magnets can be adjusted with extra screws in the rotating arms.

The rotating speed of the magnets was adjusted, controlled by a Conrad PS 405 Pro power supply. The rotation speed was calibrated with a stroboscope (LED-stroboscope HELIO-STROB micro2). A Grasshopper3 GS3-U3-23S6M high-speed camera was used to observe and record the trajectories of the particles. The 3D printed chip was designed in SolidWorks and printed with a Formlabs Form 2 printer.

The particles used in this study are magnetic Janus particles, 70–90 μm in diameter, purchased from Cospheric.[32] Their core is made of borosilicate, and they are half-coated with a superparamagnetic material.

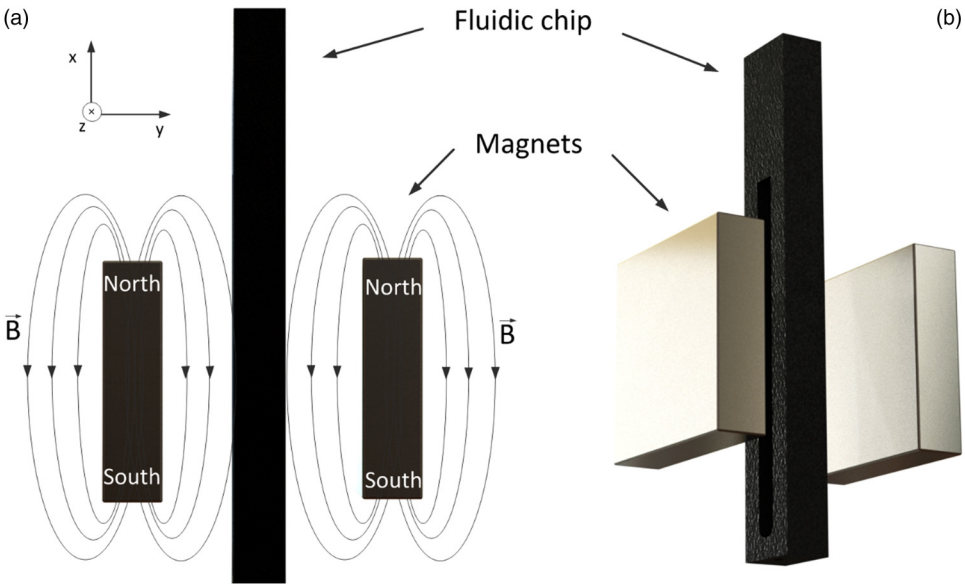

FIG. 3. (a) Schematic (side view) drawing and magnetic field distribution used to rotate the Janus particles inside the fluidic chip. (b) Diagonal view of the magnets' configuration.

Five hundred and forty-three Janus particles were placed between two 5×5 mm^2 tape layers and introduced into a Quantum Design PPMS-VSM (physical property measurement system vibrating sample magnetometer) to measure their magnetic moment. The scan rate was 1.5 mT s^{-1} from 5 T to −5 T and up to 5 T again at room temperature. Figure S4 in the supplementary material presents the experimentally obtained magnetization of the Janus particles. From the magnetization curve, it can be concluded that the Janus particles have hysteresis and that their magnetic moment saturates at ≈0.5 T, having a susceptibility of 0.06 nA m^2 T^{-1} and a remanent moment m_p of 1.5×10^{-11} A m^2 per particle.

The resulting magnetic force exerted by the magnet on the particles [Eq. (10)] was estimated from the magnet geometry using analytical integration (Cades[33]), see Sec. V in the supplementary material. We are mostly concerned with variations in the magnetic force for different particle trajectories. When the particles fall exactly along the center between the magnets, the force and force gradient is zero. If particles rotating both directions start falling at the same point, a constant force will merely cause an offset that is canceled by measuring the difference between clockwise and anti-clockwise rotation. However, in each experiment, particles rotating both sides had a small difference in position close to 1 mm due to the inaccuracy of the focusing system. Magnetic forces in the z-direction depending on z-position (z = 0.1, 1, and 5 mm) range from 0.1 to 35 pN [see Fig. S5(a) in the supplementary material]. Even particles flowing 2 mm away from the magnetic field center (x,y,z) = (0,0,0) have a force difference close to 10 pN [see Fig. S5 (b) in the supplementary material]. The gradient of the magnetic force in the z-direction, so in the same direction as the Magnus force, was estimated to be $7.5z_0$ nN/m (see Fig. S6 in the supplementary material), where z_0 is the off-center position. Therefore, particles rotating 1 mm apart had a difference in force of 7.5 pN. The magnetic attraction by the magnets is, therefore, of the same magnitude as the Magnus force itself, which is in the order of 6 pN [de-ionized (DI) water with $\mu_f = 1$ mPa s and 5 rps]. This suggests that the deflection caused by the Magnus effect is enhanced by the magnetic force. Typical deflection differences due to the Magnus effect are less than 0.1 mm, resulting in maximum magnetic force differences of 0.75 pN.

Two solutions were used, DI water and a mix of glycerol and water in a 1:3 volume ratio. Three pipet tips were glued in the three inlets to facilitate the introduction of liquids and particles. The chip was filled with a pipet until the liquid reached the top of the pipet tips. Matlab was used to track the particle trajectories, and Cades was used to simulate the magnetic field and magnetic force.

Three different experiments were performed where just the liquid viscosity and the rotation speed of the particles were modified. The experimental procedure consisted of different steps. First, the rotation of the magnets was set to a given angular speed. Second, the Janus particles were introduced in the fluidic chip via a pipet. Thereafter, they rolled and fell into the main channel at $u \approx 0.01$ m/s. Third, their trajectories over 1 cm length inside the fluidic system were recorded and subsequently analyzed. Six different steps in each experiment were performed, three clockwise and three anti-clockwise. The center of the trajectories was manually centered at 0 in order to visualize the difference between experiments.

IV. RESULTS AND DISCUSSION

Figure 4 shows the experimentally obtained angles of the trajectories of the particles and their cumulative distribution function (CDF) assuming normal distributions. In Fig. 4(a), a clear difference can be observed between particle trajectories when the magnet is rotating either clockwise or anti-clockwise, when we used water ($\upsilon_f = 1.0 \times 10^{-6}$ m^2/s), and 5 rps as angular speed, meaning $R_e \approx 1$ and $R_o = 0.2$. The deflection of the trajectories agrees with the theory: particles rotating clockwise moved to the left, and particles

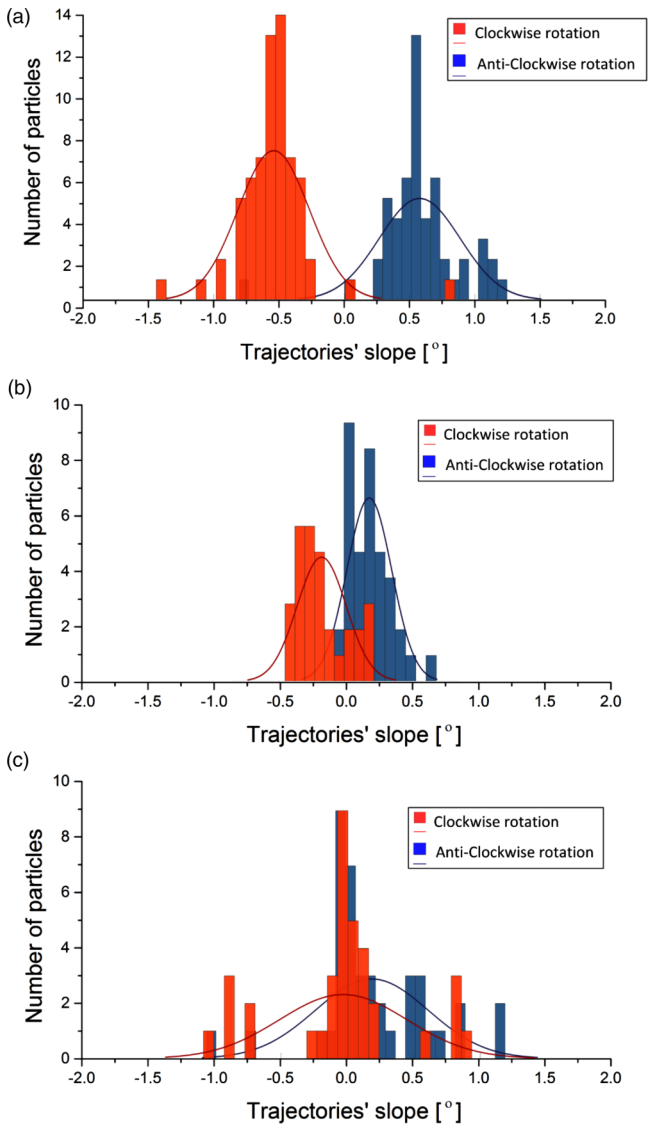

FIG. 4. Histograms and their cumulative distribution function (CDF) of the trajectory slope angles in the z-direction of particles rotating clockwise (red) and anti-clockwise (blue) (a) with low viscosity (water) and 5 rps, (b) low viscosity (water) and 2 rps, and (c) high viscosity (mix of water and glycerol 3/1 v/v) and 2 rps.

rotating anti-clockwise moved to the right. The experimental difference between the mean deflection angles for the two rotation directions was $1.2 \pm 0.3°$. This is within the error margin in agreement with the calculated angle difference of 1.2° [Eq. (9)]. Figure 4(b) shows the same experiment but using 40% of the angular speed (2 rps). The measured angle difference ($0.42 \pm 0.15°$) again agrees with the calculated angle of 0.49°. When we used a liquid with more than twice the viscosity ($\upsilon_f = 2.3 \times 10^{-6}\,m^2/s$), meaning $R_e \approx 0.2$ and $R_o = 0.03$, and low angular speed(2 rps), the difference between particles rotating in both directions drops below the measurement error. This was an expected result since the calculated angle dropped until 0.21°. When we increased the angular velocity to 5 rps, most of the particles were no longer able to follow the magnetic field rotation. Assuming the magnetic field to be in the order of 122 mT, the maximum rotation velocity in the high-viscosity medium ($\mu = 2.3$ mPa s) is, according to Eq. (2), in the order of 78 rps, so we should have observed the particles completely following the magnetic field and a deflection similar to 0.52°. We speculate that most of the particles did not have enough magnetic material and, therefore, not enough torque to follow the magnetic field.

In order to obtain larger deflections and more feasible sorting systems, larger rotation speeds are needed, which can be obtained by increasing the magnetic field strength inside the fluidic system by placing the magnets closer together. It should be noted that the Magnus force is smaller than typical magnetic forces on microparticles in microfluidic devices. Comparing different systems using magnetic fields to sort particles, it can be observed that similar forces are accomplished (1–35 pN), however, with smaller particles (1–7.3 μm).[34–39] The experimental system was constructed for minimal magnetic field gradients, and therefore required big magnets. The size can be optimized, however, especially if we allow magnetic field gradients on top of the Magnus force for additional sorting

V. CONCLUSION

In conclusion, we made magnetic Janus particles of 80 μm diameter fall through a liquid with varying viscosity in the presence of a rotating magnetic field with varying angular velocity. The Reynolds number for the particle movement was ≈1. Below a threshold field, the particles rotated with the field. These rotating particles were, therefore, subject to a Magnus force that caused a measurable tilt of up to 1.2° in their trajectories. The direction of the tilt agrees with the rotation direction and with a simple model based on the Rubinow and Keller approximation for the Magnus force at low Reynolds numbers combined with linear viscous drag. The tilt angle increased with increasing rotation velocity and decreasing kinematic viscosity. The minimum field value for rotation increases with increasing rotation velocity and viscosity of the medium. Most of the particles no longer followed a magnetic field of 122 mT in a medium with a kinematic viscosity of $2.3 \times 10^{-6}\,m^2/s$ at a rotation velocity of 5 rps and, therefore, no longer showed a tilt.

The experiments clearly demonstrate that the Magnus force on particles with a diameter of tens of micrometers is measureable. The method allows for separation of particles based on the ratio between their magnetic moment and radius to the third power.

SUPPLEMENTARY MATERIAL

See the supplementary material for the setup, the zigzag focusing system, the magnetic field rotation 3D drawing, the magnetic moment of the Janus particles and the magnetic force on the particles are shown.

ACKNOWLEDGMENTS

This work was supported by The Netherlands Centre for Multiscale Catalytic Energy Conversion (MCEC), an NWO Gravitation programme funded by the Ministry of Education, Culture and Science of the government of The Netherlands.

REFERENCES

[1]G. Magnus, "Liber die Abweichung der Geschlosse, und eine auffallende Erscheinung bei rotierenden Korpern," Ann. Phys. **88**, 1 (1853).
[2]J. R. Kensrud, "Determining aerodynamic properties of sports balls in situ," Master's thesis (Washington State University, 2010).
[3]J. C. Forbes, "Curveballs in protoplanetary discs: The effect of the Magnus force on planet formation," Mon. Not. R. Astron. Soc. **453**, 1779–1792 (2015).
[4]P. C. Rem, N. Fraunholcz, and E. A. Schokker, "Magnus separation," Sep. Sci. Technol. **37**, 3647–3660 (2002).
[5]S. I. Rubinow and J. B. Keller, "The transverse force on a spinning sphere moving in a viscous fluid," J. Fluid Mech. **11**, 447–459 (1961).
[6]M. Yamada and M. Seki, "Microfluidic particle sorter employing flow splitting and recombining," Anal. Chem. **78**, 1357–1362 (2006).
[7]X. Lu and X. Xuan, "Continuous microfluidic particle separation via elasto-inertial pinched flow fractionation," Anal. Chem. **87**, 6389–6396 (2015).
[8]D. Huh *et al.*, "Gravity-driven microfluidic particle sorting device with hydrodynamic separation amplification," Anal. Chem. **79**, 1369–1376 (2007).
[9]G. M. Whitesides, "The origins and the future of microfluidics," Nature **442**, 368–373 (2006).
[10]D. R. Gossett *et al.*, "Label-free cell separation and sorting in microfluidic systems," Anal. Bioanal. Chem. **397**, 3249–3267 (2010).
[11]H. Amini, W. Lee, and D. Di Carlo, "Inertial microfluidic physics," Lab Chip **14**, 2739–2761 (2014).
[12]C. Wyatt Shields IV, C. D. Reyes, and G. P. López, "Microfluidic cell sorting: A review of the advances in the separation of cells from debulking to rare cell isolation," Lab Chip **15**, 1230–1249 (2015).
[13]P. Sajeesh and A. Kumar Sen, "Particle separation and sorting in microfluidic devices: A review," Microfluid. Nanofluid. **17**, 1–52 (2014).
[14]H. A. Svahn and A. Van Den Berg, "Single cells or large populations?," Lab Chip **7**, 544–546 (2007).
[15]P. Li *et al.*, "Acoustic separation of circulating tumor cells," Proc. Natl. Acad. Sci. U.S.A. **112**, 4970–4975 (2015).
[16]M. Solsona *et al.*, "Magnetophoretic sorting of single catalyst particles," Angew. Chem. Int. Ed. **57**, 10589–10594 (2018).
[17]C. P. Moerland, L. J. V. Ijzendoorn, and M. W. J. Prins, "Rotating magnetic particles for lab-on-chip lab on a chip applications—A comprehensive review," Lab Chip **19**, 919–933 (2019).
[18]Y. Gou, Y. Jia, P. Wang, and C. Sun, "Progress of inertial microfluidics in principle and application," Sensors **18**, 1762 (2018).
[19]P. G. Saffman, "The lift on a small sphere in a slow shear flow," J. Fluid Mech. **22**, 385 (1965).
[20]J. Zhang *et al.*, "Fundamentals and applications of inertial microfluidics: A review," Lab Chip **16**, 10–34 (2016).

[21]M. Solsona *et al.*, "Microfluidics and catalyst particles," Lab Chip **19**, 3575–3601 (2019).
[22]H. M. Barkla and L. J. Auchterlonie, "The Magnus or Robins effect on rotating spheres," J. Fluid Mech. **47**, 437–447 (1971).
[23]J. Seifert, "A review of the Magnus effect in aeronautics," Prog. Aerosp. Sci. **55**, 17–45 (2012).
[24]P. Bagchi and S. Balachandar, "Effect of free rotation on the motion of a solid sphere in linear shear flow at moderate Re," Phys. Fluids **14**, 2719–2737 (2002).
[25]T. Kray, J. Franke, and W. Frank, "Magnus effect on a rotating sphere at high Reynolds numbers," J. Wind Eng. Ind. Aerodyn. **110**, 1–9 (2012).
[26]D. Beck, *Magnus Force Acting Upon a Rotating Sphere Passing in an Incompressible Viscous Flow* (Charles University, 2018).
[27]B. Oesterle and T. B. Dinh, "Experiments on the lift of a spinning sphere in a range of intermediate Reynolds numbers," Exp. Fluids **25**, 16–22 (1998).
[28]Y. Tsuji, Y. Morikawa, and O. Mizuno, "Experimental measurement of the Magnus force on a rotating sphere at low Reynolds numbers," J. Fluids Eng. **107**, 484 (1985).
[29]S. I. Denisov, T. V. Lyutyy, V. V. Reva, and A. S. Yermolenko, "Temperature effects on drift of suspended single-domain particles induced by the Magnus force," Phys. Rev. E **97**, 32608 (2018).
[30]C. H. Berg, *Random Walks in Biology* (Princeton University Press, 1993).
[31]See https://www.supermagnete.de/eng/block-magnets-neodymium/block-magnet-40mm-10mm-10mm_Q-40-10-10-N for for the 8 magnets used to rotate the particles.
[32]See https://www.cospheric.com/Paramagnetic_coated_glass_microspheres for the janus magnetic particles purchased.
[33]See http://www.g2elab.grenoble-inp.fr/fr/recherche/cades-1 for the software used to simulate the manetic field and force.
[34]E. Mirowski, J. Moreland, A. Zhang, S. E. Russek, and M. J. Donahue, "Manipulation and sorting of magnetic particles by a magnetic force microscope on a microfluidic magnetic trap platform," Appl. Phys. Lett. **86**, 243901 (2005).
[35]Y.-C. Chung, P.-W. Chen, C.-M. Fu, and J.-M. Wu, "Particles sorting in micro-channel system utilizing magnetic tweezers and optical tweezers," J. Magn. Magn. Mater. **333**, 87–92 (2013).
[36]Y.-C. Chung, C.-M. Wu, and S.-H. Lin, "Particles sorting in micro channel using designed micro electromagnets of magnetic field gradient," J. Magn. Magn. Mater. **407**, 209–217 (2016).
[37]T. F. Kong *et al.*, "An efficient microfluidic sorter: Implementation of double meandering micro striplines for magnetic particles switching," Microfluid. Nanofluid. **10**, 1069–1078 (2011).
[38]T. Zhu *et al.*, "Continuous-flow ferrohydrodynamic sorting of particles and cells in microfluidic devices," Microfluid. Nanofluid. **13**, 645–654 (2012).
[39]C. Liu, T. Stakenborg, S. Peeters, and L. Lagae, "Cell manipulation with magnetic particles toward microfluidic cytometry," J. Appl. Phys. **105**, 102014 (2009).